Arabian Journal of Chemistry (2023) **16**, 104915

King Saud University

Arabian Journal of Chemistry

www.ksu.edu.sa
www.sciencedirect.com

ORIGINAL ARTICLE

Preparation of HMX@DHBA-Pb and HMX@NTO-Pb composites via *in situ* deposition: A way to achieve surface catalysis of HMX

Guanchao Lan [a,b], Guanghui Gu [b], Yuchuan Wang [b], Guangyuan Zhang [b], Jianlong Wang [a], Jing Li [c,*]

[a] *School of Chemistry and Chemical Engineering, North University of China, Taiyuan 030051, China*
[b] *Gansu Yin Guang Chemical Industry Group Co. Ltd., Baiyin 730900, China*
[c] *School of Materials Science and Engineering, North University of China, Taiyuan 030051, China*

Received 9 February 2023; accepted 10 April 2023
Available online 17 April 2023

KEYWORDS

HMX;
Composites;
In situ deposition;
Catalytic

Abstract In order to ameliorate the combustion properties of 1,3,5,7-tetranitro-1,3,5,7-tetrazacyclooctane (HMX) based composite modified double base (CMDB) propellants, HMX particles with many gullies are first prepared, and then 2,4-dihydroxybenzoic acid (DHBA) and 1,2,4-triazol-5-one (NTO) are used to react with lead via *in situ* deposition to coat HMX for preparing HMX@DHBA-Pb and HMX@NTO-Pb composites. The structures and properties of HMX@DHBA-Pb and HMX@NTO-Pb composites are characterized in detail. The characterization results show that DHBA-Pb and NTO-Pb shells are uniformly coated on HMX surfaces. The chemical structure of HMX maintains constant during *in situ* deposition coating process. The mechanical and thermal safeties of HMX are enhanced after coating with DHBA-Pb and NTO-Pb shells. The introduce of DHBA-Pb and NTO-Pb can catalyze the decomposition and combustion of HMX core, and the catalytic effects of *in situ* coating are better than that of physical mixing.

1. Introduction

Solid propellant can release energy rapidly and produce a large amount of high temperature gas when burning (Song et al., 2020; Chaturvedi and Dave, 2019), which is the power source of missile and rocket engine (Zhang et al., 2022; Dubey et al., 2012). To meet the demands of high energy and low signature in solid propellants, high energy explosive are added into the formulation to prepare composite modified double base (CMDB) propellants (Elbasuney et al., 2017; Liu et al., 2018; Damse et al., 2007). 1,3,5,7-Tetranitro-1,3,5,7-tetrazacyclooctane (HMX, Fig. 1a) is one of the most commonly used high energy explosives to prepare CMDB propellants, because of the

* Corresponding author.
E-mail address: 20210064@nuc.edu.cn (J. Li).
Peer review under responsibility of King Saud University.

Production and hosting by Elsevier

https://doi.org/10.1016/j.arabjc.2023.104915

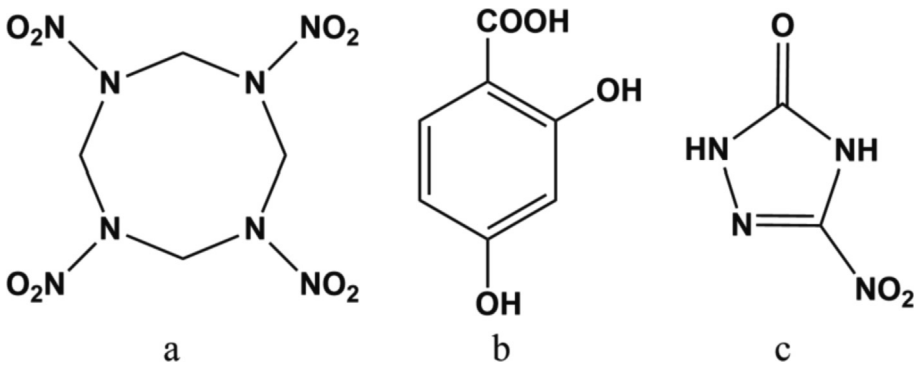

Fig. 1 Molecular structure of HMX (a), DHBA (b) and NTO (c).

excellent energetic characteristics of HMX (density 1.96 g·cm^{-3}, detonation velocity 9100 m·s^{-1}, thermal decomposition temperature 276 °C) (Klapötke, 2018; Kosareva et al., 2022). The addition of high energy explosive can not only increase the energy level, but also endows CMDB propellants with controllable signature (Liu et al., 2018; Stepanov et al., 2013). However, low burning rate and high pressure exponent are two shortcomings of CMDB propellants containing high energy explosive. Relevant studies show that organic lead salt is an effective catalyst that can improve the burning rate and adjust the pressure exponent of CMDB propellants (Liu et al., 2001; Jiang et al., 2020). Among which 2,4-dihydroxybenzoic acid (DHBA, Fig. 1b) lead and 3-nitro-1,2,4-triazol-5-one (NTO, Fig. 1c) lead are commonly used catalysts for ameliorating burning rate and pressure exponent of CMDB propellants (Yuan et al., 2014; Li et al., 1993).

In traditional CMDB propellants, the catalyst is added by physical mixing that may result in non-uniform mixing between catalyst and HMX. Moreover, in traditional CMDB propellants, HMX and catalyst are separated by adhesives and other components, *i.e.* HMX crystals are not contact with catalysts directly. Therefore, the catalytic effect of catalysts can not be sufficiently exploited in traditional CMDB propellants. In order to meet the the demands of burning rate and pressure exponent, large amounts of catalysts are added to traditional CMDB propellants, which will decrese the energy of CMDB propellants. *In situ* reaction coating technology can introduce catalysts to HMX surface by chemical reaction occurred on HMX surface. Compared with physical mixtures, *in situ* reaction can compactly and uniformly assemble catalysts on the surface of HMX, which can effectively improve the catalytic effect of catalysts. In addition, *in situ* deposition coating needs less adhesives compared with physical mixing, and thus possesses higher energy. Moreover, *in situ* deposition coating technique can facilitate extraordinarily high coverage and shell strength owing to the chemical reaction (Chaturvedi and Dave, 2019), which may enhance thermal stability and decrease mechanical sensitivity of HMX. *In situ* coating technology has been successfully applied to modify aluminum, cyclotrimethylenetrinitramine (RDX), hexanitrohexaazaisowurtzitane (CL-20) and HMX, *etc* (Li et al., 2020; Yang et al., 2015; Lan et al., 2022; Xiao et al., 2021; Xiao and Liang, 2021; Gong et al., 2017; He et al., 2018; Zhao and Zhang, 2011; Wu et al., 2008). Previous studies focus on *in situ* polymerization coating; to enhance thermal stability and decrease mechenical sensitivity of energetic materials (Li et al., 2020; Yang et al., 2015; Sánchez-Martín et al., 2011; Sun, 1998), while it is hardly to achieve surface catalytic by *in situ* polymerization coating. *In situ* deposition is an effective methods to achieve surface modification that can significantly improve the property of materials (Gao et al., 2022; Guo et al., 2023; Zhang et al., 2023; Han et al., 2022; Ren et al., 2023).

Many materials can be used as *in situ* reaction candidates to react with lead ion for coating HMX, such as DHBA and NTO, *etc*. DHBA contains two hydroxyl groups and one carboxyl group, which can easily react with Pb^{2+} to form DHBA-Pb salt under alkaline conditions (Hong et al., 2005). NTO contains two acylamino that can easily coordinate with Pb^{2+} to form NTO-Pb salt under alkaline conditions (Singh et al., 2002). The *in situ* reaction formed DHBA-Pb salt and NTO-Pb salt will precipitate from the solution and deposite on HMX surface to form HMX@DHBA-Pb and HMX@NTO-Pb composites due to the interaction between organic lead salt and HMX surface. The content of organic lead salt can be controlled by *in situ* deposition coating times. In addition, compared with pure HMX, the specific surface areas of composites are much higher and thus the adhesive accessible areas are higher, resulting in better mechanical properties.

In this study, HMX@DHBA-Pb and HMX@NTO-Pb composites are first prepared via *in situ* deposition coating process to achieve surface catalytic and enhance safety of HMX. In order to ameliorate coating effects of DHBA-Pb and NTO-Pb shells on HMX surfaces, roughening treatments are performed to obtain HMX particles with high specific surface area. The performance of HMX@DHBA-Pb and HMX@NTO-Pb composites are compared with physical mixtures of HMX/DHBA-Pb and HMX/NTO-Pb to study the catalytic effects of *in situ* deposition coating process and physical mixing.

2. Experimental details

2.1. Materials

HMX and NTO, provided by Gansu Yin Guang Chemical Industry Group Co. Ltd, were purified by recrystallization, and their mass fraction purity was greater than 0.99. 2,4-Dihydroxybenzoic acid, N,N-dimethylformamide (DMF), acetic acid, sodium laurylsulfonate, lead nitrate and sodium hydroxide were analytical grade and purchased from a local reagent factory without further purification.

2.2. Preparation of spherical HMX with high specific surface area

Generally, the surface of HMX crystals is smooth, and lead salts particles are difficult to adsorb on the surface of HMX. However, HMX particles with many gullies are benefit for the adsorption of lead salts during *in situ* deposition. HMX-DMF complex can be easily obtained through recrystallization, and the DMF of HMX-DMF complex can be easily removed through stirring in water (Ren, 1994). HMX with high specific surface area can be obtained by removing DMF in HMX-DMF complex. In order to obtain spherical HMX, some additives such as acetic acid, sodium laurylsulfonate

and water are added during the recrystallization of HMX in DMF.

100 g HMX samples and 1000 mL DMF were added into 2500 mL four-necks flask with mechanical stirring, condenser and thermometer. The suspension was heated to 85 °C and stirred at this temperature until HMX particles are completely dissolved. Then, 3.0 g sodium laurylsulfonate and 200 mL acetic acid were added into the above solution and stirring at 85 °C until the suspension became clearly transparent. Subsequently, drip 100 mL deionized water into the resulted solution and stir for 30 min at 85 °C. Then, some seed crystals were added when the solution was cooled to 80 °C and stirring for 2 h at 80 °C. Then, cool the suspension to 20 °C with a cooling rate of 2.5 °C·h^{-1}. The suspension was filtered and washed with deionized water to remove the sodium laurylsulfonate and solvent. The transparent spherical HMX-DMF complexes (Fig. 2a) with smooth surfaces were obtained. The average particle size of HMX-DMF complexes was 287.86 μm (Fig. 2b). Then, add the obtain spherical HMX-DMF complexes and 1000 mL deionized water into 2500 mL four-necks flask and heat to 50 °C stirring for 60 min to remove the DMF of HMX-DMF complexes. Then, the spherical HMX particles with high specific surface area obtained. The average particle size of the obtained HMX particles was 258.66 μm. Many gullies and holes will appear when DMF are removed. The gullies and holes are ideal adsorption sites for *in situ* deposition coating.

2.3. Preparation of HMX@DHBA-Pb and HMX@NTO-Pb composites

2.3.1. Preparation of HMX@DHBA-Pb composites

At 25 °C, 1 g DHBA samples and 100 mL deionized water were added into 250 mL three-necks flask and stirred at this temperature until DHBA are completely dissolved. Then, 20 g HMX crystals were added to DHBA solution and stirred for 30 min to disperse. Then, 500 mg $Pb(NO_3)_2$ was added to the above suspension and stirred for 30 min to supply Pb^{2+}. NaOH solution was then dripped into the above suspension to adjust the pH value to 6–7 (the color of the suspension changed to light pink). The resulted suspension was stirred at 25 °C for 1 h and then filtered and washed with deionized water to remove the unreacted DHBA and $Pb(NO_3)_2$. The obtained HMX@DHBA-Pb composites samples were dried in a vacuum oven at 50 °C for 8 h. Repeat above procedures several times to increase the mass fraction of DHBA-Pb shell to 2%. The average particle size of the obtained HMX@DHBA-Pb composites was 267.46 μm.

2.3.2. Preparation of HMX@NTO-Pb composites

At 25 °C, 1 g NTO samples were dissolved in 100 mL deionized water and then 20 g HMX crystals were added to NTO solution and stirred for 30 min to disperse. Then, 500 mg Pb $(NO_3)_2$ was added to the above suspension and stirred for 30 min to supply Pb^{2+}. NaOH solution was then dripped into the above suspension to adjust the pH value to 5–6 (the color of the suspension changed from yellow-green to light yellow). The resulted suspension was stirred at 25 °C for 1 h and then filtered and washed with deionized water to remove the unreacted NTO and $Pb(NO_3)_2$. The obtained HMX@NTO-Pb composites samples were dried in a vacuum oven at 50 °C for 8 h. Repeat above procedures several times to increase the mass fraction of NTO-Pb shell to 2%. The average particle size of the obtained HMX@DHBA-Pb composites was 274.37 μm.

2.4. Characterization of HMX@DHBA-Pb and HMX@NTO-Pb composites

The structure of HMX@DHBA-Pb and HMX@NTO-Pb composites were characterized by X-ray photoelectron spectroscopy (XPS), X-ray diffraction (XRD) and Fourier-transform infrared spectra (FT-IR) respectively. The surface morphology and surface roughness of HMX@DHBA-Pb and HMX@NTO-Pb composites were investigated by scanning electron microscope (SEM) and atomic force microscope (AFM). Mechanical sensitivities of HMX@DHBA-Pb and HMX@NTO-Pb composites were measured to study the amelioration effects of DHBA-Pb and NTO-Pb shells on HMX mechanical safety. Differential scanning calorimetry (DSC) was used to study the non-isothermal decomposition properties of HMX@DHBA-Pb and HMX@NTO-Pb composites. Accelerating rate calorimeter (ARC) was used to study the catalytic effects of DHBA-Pb and NTO-Pb on HMX thermal

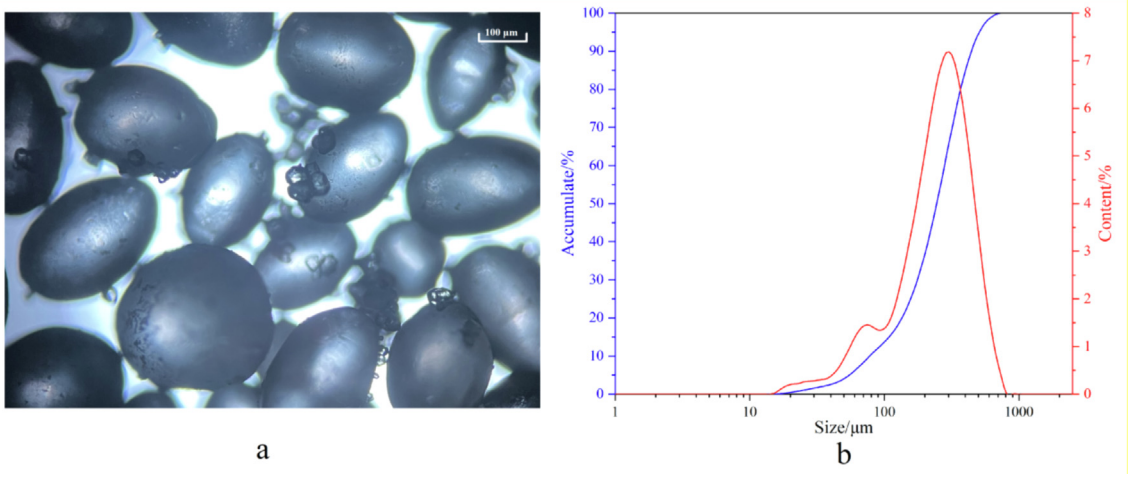

Fig. 2 Crystal morphology (a) and particle size distribution (b) of spherical HMX-DMF complex.

decomposition. The combustion residues are collected and characterized by energy dispersive spectroscopy (EDS), XRD and XPS to further study the catalytic effect of lead salt shells.

3. Results and discussions

3.1. Structure characterization of HMX@DHBA-Pb and HMX@NTO-Pb composites

3.1.1. Surface element analysis and crystal structure of HMX@DHBA-Pb and HMX@NTO-Pb composites

The surface element of HMX, HMX@DHBA-Pb and HMX@NTO-Pb are characterized by XPS to confirm the effectiveness of *in situ* coating process. The element types of DHBA-Pb and NTO-Pb shells are different with core (HMX). Therefore, we can judge whether DHBA-Pb or NTO-Pb shell coated to the surface of HMX by element types using XPS. Full XPS spectra of different samples are listed in Fig. 3a. It can be seen from Fig. 3a that all of the main peaks of pure HMX can be indexed to C1s, N1s, and O1s electrons exclusively, which originates from HMX crystal. For HMX@DHBA-Pb and HMX@NTO-Pb composites, Pb4f peak is detected in XPS survey spectra, which are originated from DHBA-Pb and NTO-Pb. The existence of Pb4f peak demonstrates that DHBA-Pb and NTO-Pb may deposit on the surface of HMX. In addition, the high-resolution spectra of core (HMX) and shell (DHBA-Pb and NTO-Pb) show distinct differences. Therefore, high-resolution spectra of XPS can be used to further confirmation of the surface structure of different samples. The high-resolution XPS spectrum of C1s region of HMX, HMX@DHBA-Pb and HMX@NTO-Pb are shown in Fig. 3b. C1s region of HMX can be divided into two peaks, assigned to C–H (284.68 eV) and N-C-N (287.48 eV). The peak shapes of C1s of HMX@DHBA-Pb and HMX@NTO-Pb have some differences with HMX, for example the intensity of the peak around 284 eV are increased because of the introduce of C–C and C–H on HMX surfaces. The variations of high-resolution spectrum illustrate that the surface element has been changed after coating. The emergence of Pb4f peaks and the variation of C1s peaks illustrate that DHBA-Pb and NTO-Pb may deposit on the surface of HMX.

The crystal structures of HMX, HMX@DHBA-Pb and HMX@NTO-Pb are characterized by XRD and FT-IR. XRD patterns of different samples are listed in Fig. 4a. HMX showed sharp and well-defined peaks due to its crystalline structure. After coating with DHBA-Pb and NTO-Pb shells, the characteristic peaks of HMX still exist, illustrating that the crystal form of HMX are not changed. The results reflected that the crystalline phase remained stable during the coating process. FT-IR spectra of different samples are illustrated in Fig. 4b. It can be concluded from Fig. 4b that the FT-IR spectra of HMX@DHBA-Pb and HMX@NTO-Pb composites are consistent with HMX well, illustrating that the chemical structures of HMX in HMX@DHBA-Pb and HMX@NTO-Pb composites remain stable during the coating process. Due to the strong response for HMX and low content of DHBA-Pb and NTO-Pb, it is hard to detect the response of DHBA-Pb and NTO-Pb. Therefore, it can be deduced from XRD and FT-IR results that the physical and chemical properties of HMX have not changed during the coating process.

3.1.2. Coating effects of HMX@DHBA-Pb and HMX@NTO-Pb composites

XPS results show that the surface elements of HMX@DHBA-Pb and HMX@NTO-Pb composites are different with pure HMX due to the existence of DHBA-Pb and NTO-Pb shells. The coating effects of DHBA-Pb and NTO-Pb shells on HMX surfaces are further characterized by SEM, and the characterization results are shown in Fig. 5. It can be seen from Fig. 5a that the surface of HMX-DMF is smooth, as a result of the crystallization process. The surface of HMX particles with high specific surface area is displayed in Fig. 5b. There are many gullies emerged on HMX particles surfaces due to the remove of DMF during the roughening treatments of HMX. The gullies can provide many adsorption sites for lead salts, which is benefit for *in situ* deposition coating process. Fig. 5c and Fig. 5d display the surface morphology of HMX@DHBA-Pb and HMX@NTO-Pb composites, which obviously shows that DHBA-Pb and NTO-Pb shells are formed and uniformly coated on the surfaces, edges, and corners of HMX. The surface of HMX@DHBA-Pb and HMX@NTO-Pb composites are roughness due to many

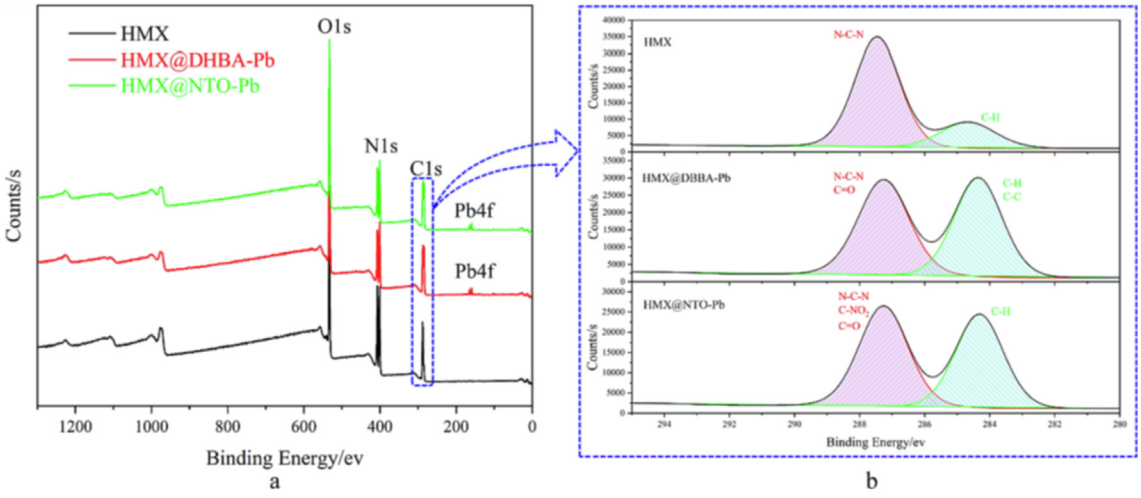

Fig. 3 Full XPS spectra (a) and C1s XPS spectra (b) of HMX, HMX@DHBA-Pb and HMX@NTO-Pb.

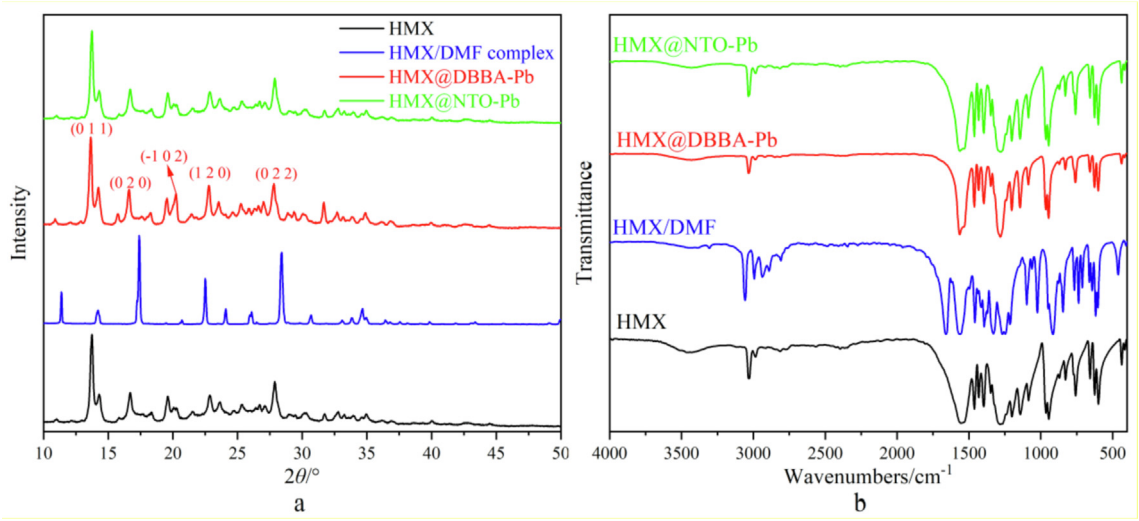

Fig. 4 XRD patterns (a) and FT-IR spectra (b) of HMX, HMX@DHBA-Pb and HMX@NTO-Pb.

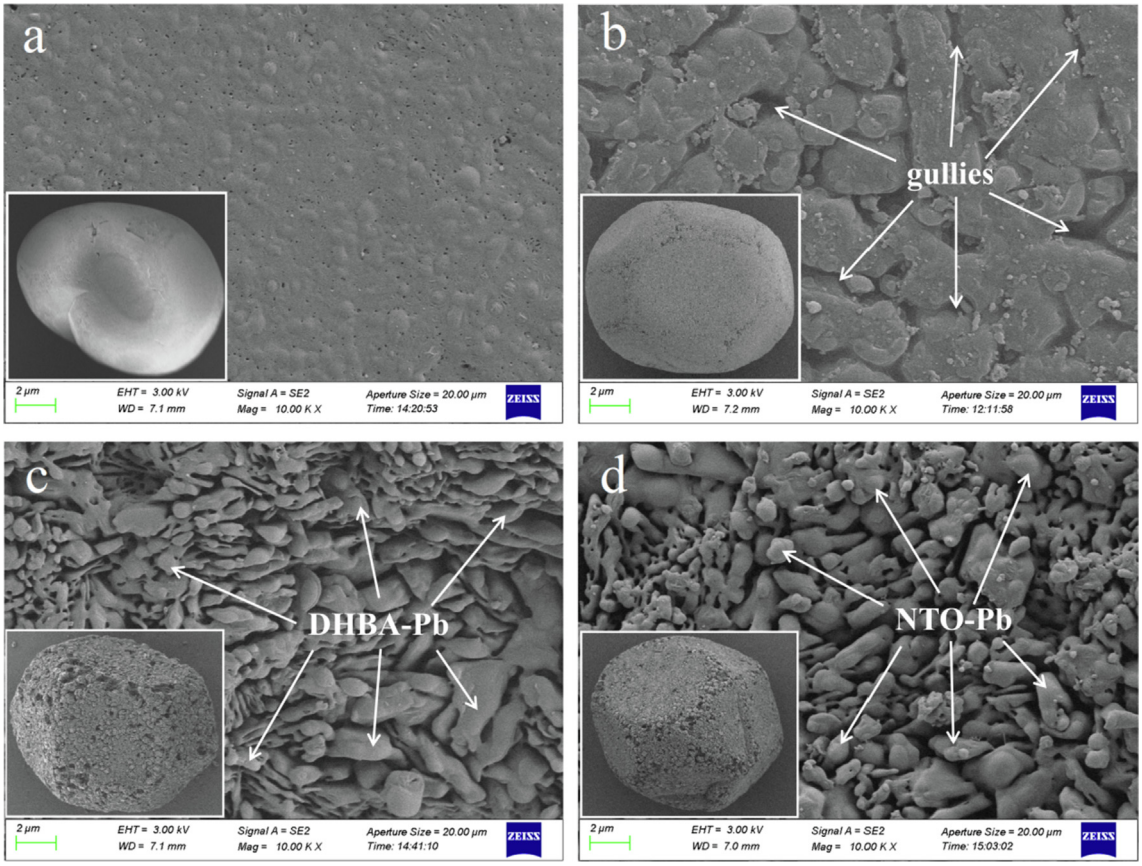

Fig. 5 Surface morphology of HMX-DMF (a), HMX particle (b), HMX@DHBA-Pb (c) and HMX@NTO-Pb (d).

DHBA-Pb and NTO-Pb particles adsorption on the surface of HMX. During *in situ* coating process, DHBA-Pb particles firstly formed in the solutions, and then adsorbed on HMX surfaces because of the non-bond interaction (hydrogen bond and van der Waals force) between DHBA-Pb particles and HMX surfaces, and so does the HMX@NTO-Pb composites. The roughness surfaces of HMX@DHBA-Pb and HMX@NTO-Pb composites can further increase the specific surface area of samples, resulting in a significant improvement of binder accessible area and thus a significant improvement of mechanical properties. The DHBA-Pb and NTO-Pb shells can protect HMX crystals when suffering external stimulations, which may ameliorate the sensitivity and thermal stability of HMX. In addition, when the energy of electron beam is high,

HMX surface easily crack and become wrinkled, while the surface of HMX@DHBA-Pb and HMX@NTO-Pb composites are much stabler under the same condition, indicating HMX crystals become obviously resistant to electronic beam under protection of DHBA-Pb and NTO-Pb shells.

3.1.3. Surface roughness of HMX@DHBA-Pb and HMX@NTO-Pb composites

SEM results show that the surface roughness of HMX@DHBA-Pb and HMX@NTO-Pb composites are much higher than that of HMX-DMF and HMX particles. The surface roughness of HMX-DMF, HMX particles, HMX@DHBA-Pb and HMX@NTO-Pb are further characterized by AFM, and the three-dimensional AFM images of different samples are presented in Fig. 6. Fig. 6a displays the topographical image of HMX-DMF surface, which illustrates that the surface of HMX-DMF is smooth and the mean value of roughness (R_a) is low (28.3 nm). Fig. 6b shows the topographical image of HMX particles after roughening treatments, which illustrates that the roughness of HMX particles is increased greatly. The R_a of HMX particles increases to 123 nm which increases 4 times compared with HMX-DMF. Fig. 6c and Fig. 6d show that the roughness of HMX@DHBA-Pb and HMX@NTO-Pb composites are markedly increased, and the topographical image of these two composites have great differences from HMX particle surface. Compared with HMX particles, the R_a of HMX@DHBA-Pb and HMX@NTO-Pb increase from 28.3 nm to 650 nm and 582 nm. It can be seen from Fig. 6c and Fig. 6d that many peaks and valleys are emerged because of the deposition and adsorption of DHBA-Pb and NTO-Pb. Combining Fig. 5 with Fig. 6, both AFM and SEM images show DHBA-Pb and NTO-Pb shells are formed and coated on the surface of HMX, and the roughness are remarkedly increased after *in situ* coating. Such improvement in surface roughness provides an additional benefit to the adhesion of HMX crystals in energetic composites, which can be utilized for further practical applications.

3.2. Performance characterizations of HMX@DBA-Pb and HMX@NTO-Pb composites

3.2.1. Mechanical sensitivities and ignition temperature of HMX@DHBA-Pb and HMX@NTO-Pb composites

XPS, SEM and AFM results illustrate that DHBA-Pb and NTO-Pb particles have been successfully coated on HMX sur-

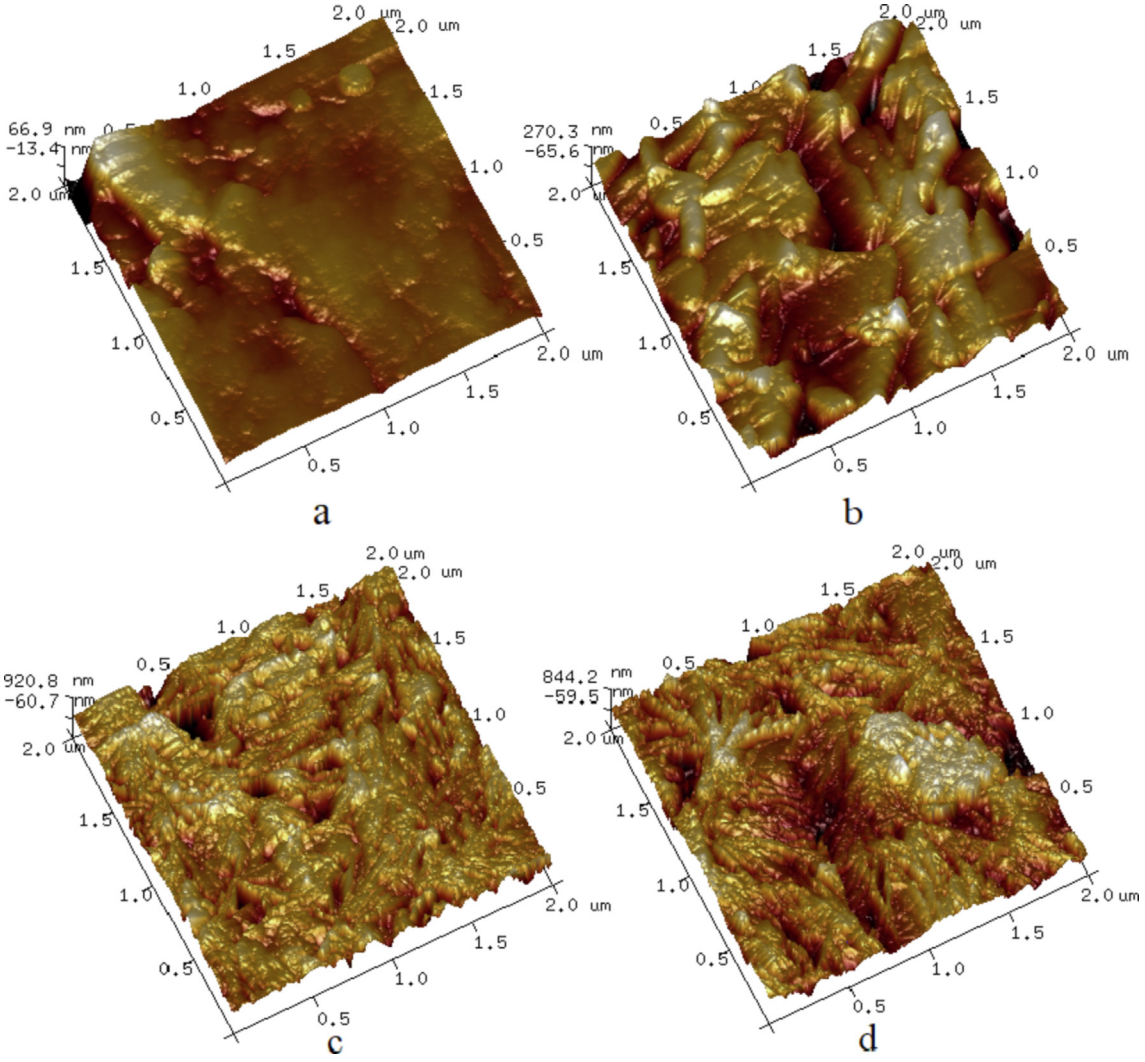

Fig. 6 Topographical AFM images of HMX-DMF (a), HMX particle (b), HMX@DHBA-Pb (c) and HMX@NTO-Pb (d).

faces and formed hard DHBA-Pb and NTO-Pb shells. The hard shells can protect the core HMX, and thus enhance the mechanical and thermal safeties of HMX. The impact sensitivity, friction sensitivity and ignition temperature (5 s delay method) of HMX particles, HMX@DHBA-Pb and HMX@NTO-Pb are measured to evaluate the influences of DHBA-Pb and NTO-Pb shells on mechanical and thermal safeties of HMX according to GJB 772A (GJB 772A, 1997). During mechanical sensitivity tests, the room temperature is 20 °C and relative humidity is 30%, and 25 samples are measured for both impact sensitivity and friction sensitivity. 30 mg sample is used to determine the impact sensitivity using a fall hammer apparatus (WL-1) with a 10 kg drop hammer and 25 cm drop height. 30 mg sample is used to determine the friction sensitivity using a pendular friction sensitivity apparatus (WM-1) with a 2 kg pendular hammer and 90° pivot angle. The obtained results are summarized in Table 1.

It can be concluded from Table 1 that the mechanical sensitivities of HMX are decreased after spheroidization treatments, in that the mechanical stimulations can evenly act on spherical HMX particles surface resulting in stress dispersion and thus decreasing the probability of hot spot formation. The mechanical sensitivities of HMX@DHBA-Pb and HMX@NTO-Pb are lower than spherical HMX particles due to the protection of DHBA-Pb and NTO-Pb shells. *In situ* deposition coating technique facilitate extraordinarily high coverage and shell strength owing to the chemical reaction occurred on the surface of HMX. High strength lead salt shells endow HMX hard armours that can protect HMX crystals when suffering external mechanical stimulations and thus decrease the mechanical sensitivities. Compared with raw HMX, the ignition temperature of spherical HMX particles, HMX@DHBA-Pb and HMX@NTO-Pb increase from 304 °C to 311 °C, 317 °C and 309 °C, illustrating that the thermal sensitivities of spherical HMX particles, HMX@DHBA-Pb and HMX@NTO-Pb are decreased. For composites, the DHBA-Pb and NTO-Pb shells can decline the heat transportation rate and absorb some heat, resulting in higher ignition temperature of HMX@DHBA-Pb and HMX@NTO-Pb. Above all, the mechanical and thermal safeties of HMX can be obviously enhanced by coating with DHBA-Pb and NTO-Pb shells.

3.2.2. Non-isothermal decomposition of HMX@DHBA-Pb and HMX@NTO-Pb composites

Ignition temperature results show that the DHBA-Pb and NTO-Pb shells have great influences on thermal properties of HMX. The non-isothermal decomposition properties of HMX@DHBA-Pb and HMX@NTO-Pb composites are further characterized by DSC at a heating rate of 10 °C·min^{-1} with nitrogen atmosphere. The obtained DSC results of pure HMX and different composites are summarized in Fig. 7a. In addition, the non-isothermal decomposition properties of HMX/DHBA-Pb and HMX/NTO-Pb physical mixtures are measured by DSC at a heating rate of 10 °C·min^{-1} with nitrogen atmosphere as well. The mass fraction of DHBA-Pb and NTO-Pb are 2%, which are the same with that of HMX@DHBA-Pb and HMX@NTO-Pb composites. The obtained DSC results of pure HMX and different physical mixtures are summarized in Fig. 7b. The melting temperature (T_m), phase transition temperature (T_t), decomposition temperature (T_p) and released heat (ΔH) of different samples are summarized in Table 2.

Fig. 7b and Table 2 illustrate that compared with pure HMX, there is no significant change in T_t, T_m, T_p and final decomposition temperature (T_f) of different physical mixtures, illustrating that physical mixing has few influences on non-isothermal decomposition properties of HMX. This phenomenon demonstrates that the catalytic effect of catalysts can not be sufficiently exploited by physical mixing. Fig. 7a illustrates that compared with pure HMX, the T_t of HMX@DHBA-Pb and HMX@NTO-Pb composites decrease from 191.17 °C to 176.83 °C and 176.50 °C, demonstrating that DHBA-Pb and NTO-Pb can catalyze the phase transition process of HMX. Ref. (Yang et al., 2015) reported that the T_t increased after *in situ* polymerization coating with melamine–formaldehyde (MF) resins, in that MF is a polymer material with outstanding heat resistant. MF shell can reduce the heat transfer rate and thus increase the T_t, and so as other *in situ* polymerization coated energetic materials (Li et al., 2020; Yang et al., 2015). DHBA-Pb and NTO-Pb are metallic salt with good thermal conductivity and Pb is a good catalyst for phase transition, and thus decrease the T_t. In addition, there is no significant change in T_m of HMX@DHBA-Pb and HMX@NTO-Pb composites, demonstrating that DHBA-Pb and NTO-Pb have few influences on the melting process of core HMX. The initial decomposition temperatures of HMX@DHBA-Pb and HMX@NTO-Pb composites are close to that of pure HMX, illustrating that the DHBA-Pb and NTO-Pb shells have few influences on thermal stability of HMX, which is similar with the results of Ref. (Li et al., 2020; Yang et al., 2015). The T_p of HMX@DHBA-Pb and HMX@NTO-Pb composites decrease from 282.83 °C to 282.35 °C and 282.22 °C, illustrating that the decomposition rate of HMX can be enhanced by the decomposition products of DHBA-Pb and NTO-Pb. The full width at half-maximum of decomposition peak decreases from 5.33 °C to 4.08 °C and 3.77 °C for HMX@DHBA-Pb and HMX@NTO-Pb, illustrating that the decomposition periods of HMX@DHBA-Pb and HMX@NTO-Pb composites are shortened and the decomposition rate is increased because of the existence of lead salt shells. Therefore, DHBA-Pb and NTO-Pb shells can catalyze the phase transition and thermal decomposition process of HMX, while DHBA-Pb and NTO-Pb shells have few influences on thermal stability of HMX. Compared with physical mixing, the catalytic effect of Pb

Table 1 Impact sensitivity, friction sensitivity and ignition temperature of HMX particles, HMX@DHBA-Pb and HMX@NTO-Pb.

parameters	raw HMX	HMX particles	HMX@DHBA-Pb	HMX@NTO-Pb
impact sensitivity/%	100	76	60	72
friction sensitivity/%	100	84	72	76
ignition temperature/°C	304	311	317	309

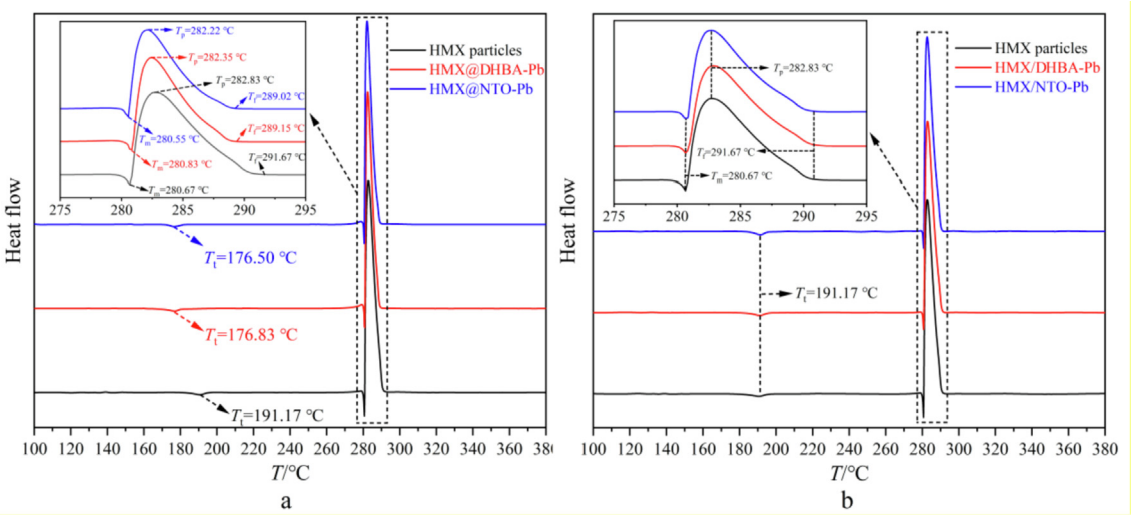

Fig. 7 A DSC results of HMX, HMX@DHBA-Pb and HMX/DHBA-Pb, b DSC results of HMX, HMX@NTO-Pb and HMX/NTO-Pb.

Table 2 The melting temperature (T_m), decomposition temperature (T_p) and released heat (ΔH) of different samples.

	HMX	HMX@NTO-Pb	HMX/NTO-Pb	HMX@DHBA-Pb	HMX/DHBA-Pb
T_m/°C	280.67	280.55	280.61	280.83	280.72
T_t/°C	191.17	176.50	191.22	176.83	191.19
T_p/°C	282.83	282.22	282.80	282.35	282.76
ΔH/(J·g^{-1})	829.80	834.73	812.65	839.46	830.16

can be exploited more sufficiently through *in situ* deposition coating.

3.2.3. Catalytic effects of DHBA-Pb and NTO-Pb shells on HMX

DSC results illustrate that DHBA-Pb and NTO-Pb shells can catalyze the thermal decomposition process of HMX. In this study, ARC is used to study the catalytic effects of DHBA-Pb and NTO-Pb shells on thermal decomposition of HMX. 120 ± 1 mg samples are measured using heat-wait-search (HWS) procedure with temperature increment of 5 °C (Lan et al., 2022; Lan et al., 2020). In addition, the adiabatic thermal decomposition period of HMX/DHBA-Pb and HMX/NTO-Pb physical mixtures are measured by ARC with the same measurement conditions as well. The obtained exothermic processes of different samples are summarized in Fig. 8. The obtained initial decomposition temperature (T_0), initial decomposition time (t_0), final decomposition temperature (T_f), final decomposition time (t_f), adiabatic temperature rise (ΔT_{ad}), maximum temperature rise rate (β_m) and whole decomposition period (Δt) are listed in Table 3.

ARC measured results demonstrate that compared with pure HMX, the T_0 of HMX/DHBA-Pb and HMX/NTO-Pb physical mixtures has few variations, while the T_0 of HMX@DHBA-Pb and HMX@NTO-Pb composites increases from 225.65 °C to 236.14 °C and 235.54 °C. These phenomena demonstrate that physical mixing has few influences on the adiabatic stability of HMX, while *in situ* deposition coating can effectively enhance the adiabatic stability of HMX. The decomposition temperatures of DHBA-Pb and NTO-Pb are lower than HMX, while ARC does not detect the decomposition process of DHBA-Pb and NTO-Pb in composites or physical mixtures because of the low content of DHBA-Pb and NTO-Pb. However, the heat resistant decomposition products generated by DHBA-Pb and NTO-Pb are compactly and uniformly assembled on the surface of HMX, and thus the adiabatic stability of HMX can be effectively enhanced. The T_0 of HMX@DHBA-Pb and HMX@NTO-Pb composites are close to each other, illustrating that the adiabatic stability of HMX@DHBA-Pb and HMX@NTO-Pb composites are close. The ΔT_{ad} of HMX@DHBA-Pb and HMX@NTO-Pb composites are higher than HMX, while the ΔT_{ad} of HMX/DHBA-Pb and HMX/NTO-Pb physical mixtures are close to HMX. These phenomena demonstrate that the decomposition reactions of HMX in HMX@DHBA-Pb and HMX@NTO-Pb composites occur more complete. Compared with pure HMX, the β_m of HMX@DHBA-Pb composites, HMX/DHBA-Pb physical mixtures, HMX@NTO-Pb composites and HMX/NTO-Pb physical mixtures increase from 753.32 °C·min^{-1} to 1510.34 °C·min^{-1}, 977.71 °C·min^{-1}, 1303.41 °C·min^{-1} and 913.58 °C·min^{-1}, and the Δt decrease from 28.88 min to 6.69 min, 14.09 min, 6.96 min and 17.16·min, respectively. These phenomena illustrate that the decomposition rates of HMX are enhanced and the total decomposition period of HMX are enhanced by DHBA-Pb and NTO-Pb. The β_m of composites are higher than that of physical mixtures and the Δt of composites are shorter than that of physical mixtures, illustrating that the catalytic effects of lead salt are better

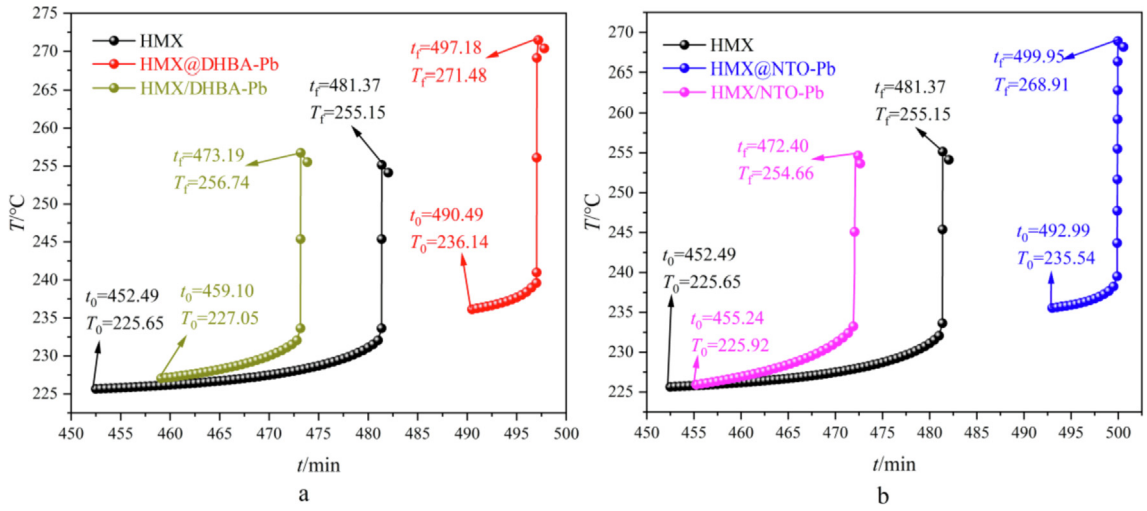

Fig. 8 A arc results of HMX, HMX@DHBA-Pb composites and HMX/DHBA-Pb physical mixtures, b ARC results of HMX, HMX@NTO-Pb composites and HMX/ NTO-Pb physical mixtures.

Table 3 Adiabatic thermal decomposition parameters of HMX, HMX@DHBA-Pb composites, HMX/DHBA-Pb physical mixtures, HMX@NTO-Pb composites and HMX/NTO-Pb physical mixtures.

parameters	HMX	HMX@DBA-Pb	HMX/DBA-Pb	HMX@NTO-Pb	HMX/NTO-Pb
sample mass/g	0.1202	0.1210	0.1209	0.1204	0.1202
T_0/°C	225.65	236.14	227.05	235.54	225.92
t_0/min	452.49	490.49	459.10	492.99	455.24
T_f/°C	255.15	271.48	256.74	268.91	254.66
t_f/min	481.37	497.18	473.19	499.95	472.40
ΔT_{ad}/°C	29.50	35.34	29.69	33.37	28.74
β_m/(°C·min^{-1})	753.32	1510.34	977.71	1303.41	913.58
Δt/min	28.88	6.69	14.09	6.96	17.16

through *in situ* deposition coating. Above all, both physical mixing and *in situ* deposition coating can catalyze the thermal decomposition process of HMX, while the catalytic effects of catalysts are better through *in situ* deposition coating.

To further study the catalytic effect of DHBA-Pb and NTO-Pb shells on the combustion of HMX in air atmosphere, HMX, HMX@DHBA-Pb composites, HMX/DHBA-Pb physical mixtures, HMX@NTO-Pb composites and HMX/ NTO-Pb physical mixtures are combusted in the air atmosphere, and then the solid residues are collected for further EDS, XRD and XPS analyses. The EDS image of the solid residues of different samples are shown in Fig. 9. The weight content of each atom of the solid residues is summarized in Table 4. Each sample is treated by spraying gold before EDS measurement resulting in the emergence of Au peak on each EDS image. After combustion, Pb peak appears on the EDS spectra of both physical mixtures and composites, and the peak intensity of composites are much higher than that of physical mixtures. Table 4 illustrates that the sum content of C, N, O of HMX residues is higher than that of physical mixtures and composites, illustrating that the combustion of physical mixtures and composites are more sufficiently due to the existence of lead salt catalysts. Take the sum content of C, N, O as criterion to assess the catalytic effect, the combustion efficiency of physical mixtures and composites approximately raise 1.4 and 2.2 times, illustrating that the catalytic effects of *in situ* coating is better.

Fig. 10 displays the XRD patterns of the solid residues of different samples after combustion. The XRD patterns of the residues of HMX/DHBA-Pb physical mixtures and HMX/ NTO-Pb physical mixtures are similar with that of pure HMX, while the intensities of the XRD patterns of the physical mixtures are lower than that of pure HMX illustrating that the catalytic effect of catalysts can not be sufficiently exploited by physical mixing. For the residues of HMX@DHBA-Pb composites and HMX@NTO-Pb composites after combustion, their XRD patterns are different with that of pure HMX and the intensities of the peaks are much lower, indicating that the combustion of HMX can be conducted thoroughly, thereby promoting the combustion efficiency of HMX. In addition, the DHBA-Pb and NTO-Pb shells coated on the surface of HMX will release some heat that will directly heat HMX crystals during the combustion, which is another reason for enhancing the combustion degree of HMX. Above all, both physical mixing and *in situ* deposition coating can catalyze the combustion of HMX, while the catalytic effects of catalysts are better through *in situ* deposition coating.

Fig. 11 displays the high-resolution XPS spectrum of O1s region of XPS spectra of the solid residues of different samples after combustion. O1s region of the solid residues of HMX can

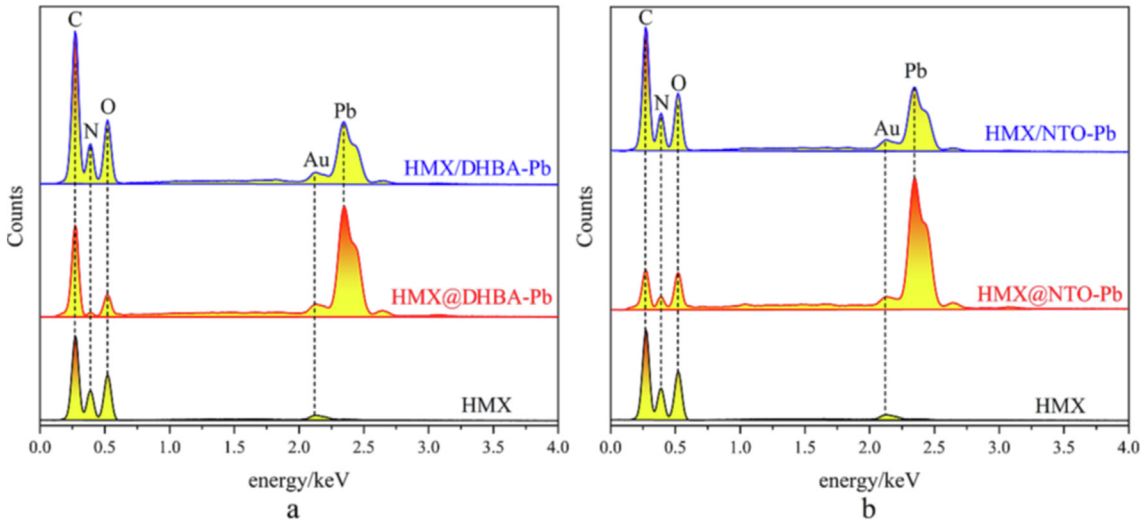

Fig. 9 A eds spectra of the residues of HMX, HMX@DHBA-Pb and HMX/DHBA-Pb, b EDS spectra of the residues of HMX, HMX@NTO-Pb and HMX/NTO-Pb.

Table 4 Weight content of the residues of HMX, HMX@DHBA-Pb, HMX/DHBA-Pb, HMX@NTO-Pb and HMX/NTO-Pb.

Element	HMX	HMX@DHBA-Pb	HMX/DHBA-Pb	HMX@NTO-Pb	HMX/NTO-Pb
C	30.83	34.69	26.55	16.20	26.30
N	33.23	2.95	24.47	9.10	24.04
O	33.94	8.53	22.38	13.30	20.80
CNO	100	46.17	73.4	38.6	71.14
Pb	/	53.83	26.60	61.39	28.86

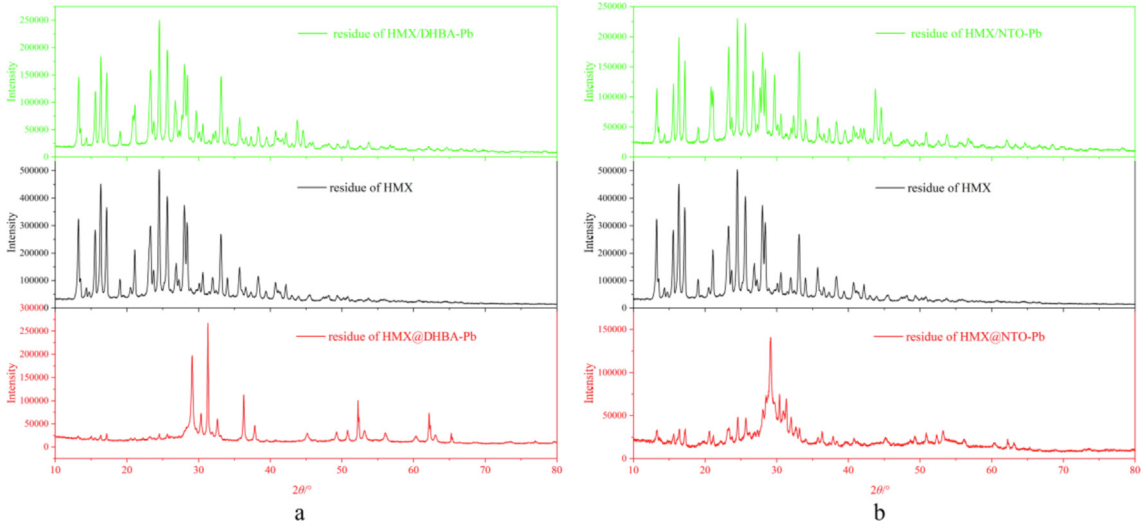

Fig. 10 A xrd patterns of the residues of hmx, hmx@dhba-pb and hmx/dhba-pb, b xrd patterns of the residues of hmx, hmx@nto-pb and hmx/nto-pb.

be divided into two peaks that can be assigned to N-O (532.58 eV) and C-O (531.38 eV). The peak shapes of O1s of both composites and physical mixtures are different with HMX, due to the emergence of Pb-O (528.38 eV). Compared with pure HMX, the intensity of C-O and N-O of composites and physical mixtures are lower, illustrating that the reaction degree of both composites and physical mixtures are higher than that of HMX. Moreover, the carbon content of

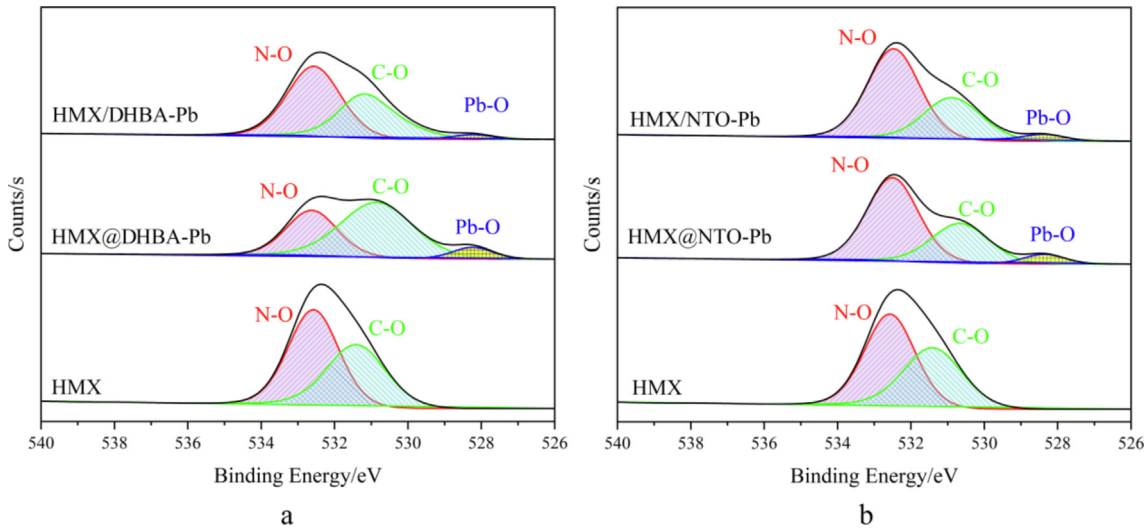

Fig. 11 A xps spectra of the residues of HMX, HMX@DHBA-Pb and HMX/DHBA-Pb, b XPS spectra of the residues of HMX, HMX@NTO-Pb and HMX/NTO-Pb.

DHBA-Pb is high resulting in an increasing of the in tensity of C-O peak. In addition, the intensity of C-O and N-O of composites are lower than that of physical mixtures, illustrating that the catalytic effects of catalysts are better through *in situ* deposition coating.

4. Conclusions

HMX@DHBA-Pb and HMX@NTO-Pb composites are prepared via *in situ* deposition coating. XPS, SEM and AFM results show that DHBA-Pb and NTO-Pb shells have compactly coated on HMX surface. XRD and FT-IR results show that the physical and chemical structures of HMX have not changed during the coating process. The mechanical and thermal sensitivities of HMX@DHBA-Pb and HMX@NTO-Pb composites are remarkedly decreased, illustrating that the safety of HMX is enhanced after coating with DHBA-Pb and NTO-Pb shells, which is the same with *in situ* polymerization coating process. DHBA-Pb and NTO-Pb shells can catalyze the phase transition of HMX, which is different with *in situ* polymerization coating process. Compared with physical mixtures, the decomposition periods of composites are shorter and the combustion are more complete, illustrating that the catalytic effects of *in situ* deposition are better than physical mixing. Above all, DHBA-Pb and NTO-Pb shells can decrease the mechanical and thermal sensitivity of HMX and catalyze the thermal decomposition of HMX. In addition, the catalytic effects of lead salts are better through *in situ* deposition coating than physical mixing.

Declaration of Competing Interest

The authors declare that they have no known competing financial interests or personal relationships that could have appeared to influence the work reported in this paper.

Acknowledgments

This work was supported by Fundamental Research Program of Shanxi Province (Grant No. 202103021223192).

References

Chaturvedi, S., Dave, P.N., 2019. Solid propellants: AP/HTPB composite propellants. Arab. J. Chem. 12, 2061–2068.

Damse, R.S., Singh, A., Singh, H., 2007. High energy propellants for advanced gun ammunition based on RDX, GAP and TAGN compositions. Propell. Explos. Pyrot. 32, 52–56.

Dubey, R., Srivastava, P., Kapoor, I.P.S., Singh, G., 2012. Synthesis, characterization and catalytic behavior of Cu nanoparticles on the thermal decomposition of AP, HMX, NTO and composite solid propellants. Thermochim. Acta 549, 102–109.

Elbasuney, S., Fahd, A., Mostafa, H.E., 2017. Combustion characteristics of extruded double base propellant based on ammonium perchlorate/aluminum binary mixture. Fuel 208, 296–304.

Gao, M., Tian, F., Guo, Z., Zhang, X., Li, Z., Zhou, J., Zhou, X., Yu, Y., Yang, W., 2022. Mutual-modification effect in adjacent Pt nanoparticles and single atoms with sub-nanometer inter-site distances to boost photocatalytic hydrogen evolution. Chem. Eng. J. 446, 137127.

GJB 772A, Explosive test method, Beijing, China Weapons Industry Press, 1997.

Gong, F.Y., Zhang, J.H., Ding, L., Yang, Z.J., Liu, X.B., 2017. Mussel-inspired coating of energetic crystals: A compact core-shell structure with highly enhanced thermal stability. Chem. Eng. J. 309, 140–150.

Guo, X., Li, M., Qiu, L., Tian, F., He, L., Geng, S., Liu, Y., Song, Y., Yang, W., Yu, Y., 2023. Engineering electron redistribution of bimetallic phosphates with CeO_2 enables high-performance overall water splitting. Chem. Eng. J. 453, 139796.

Han, G., Li, M., Liu, H., Zhang, W., He, L., Tian, F., Liu, Y., Yu, Y., Yang, W., Guo, S., 2022. Short-range diffusion enables general synthesis of medium-entropy alloy aerogels. Adv. Mater. 34, 2202943.

He, W., Liu, P., Gong, F., Tao, B., Gu, J., Yang, Z., Yan, Q., 2018. Tuning the reactivity of metastable intermixed composite n–Al/PTFE by polydopamine interfacial control. ACS Appl. Mater. Interfaces 10, 32849–32858.

Hong, W.L., Liu, J.H., Qiu, C.E., Zhao, F.Q., Tian, D.Y., Zhang, P. X., Wang, F., 2005. Synthesis and combustion catalytic activity of nanoparticle Pb(Ⅱ)-resorcylic acid complex. Chem. J. Chinese U. 26, 889–893.

Jiang, Q., Luo, Y., Yang, F., Ju, R., Zhang, M., Wang, W., Li, B., 2020. Influence of lead and copper salt catalysts on the thermal decomposition and cook-off responses of DNTF. Chin. J. Energ. Mater. 28, 470–474.

Klapötke, T.M., 2018. Energetic Materials Encyclopedia. De Gruyter, Berlin.

Kosareva, E.K., Zharkov, M.N., Meerov, D.B., Gainutdinov, R.V., Fomenkov, I.V., Zlotin, S.G., Pivkina, A.N., Kuchurov, I.V., Muravyev, N.V., 2022. HMX surface modification with polymers via sc-CO2 antisolvent process: a way to safe and easy-to-handle energetic materials. Chem. Eng. J. 428, 131363.

Lan, G., Jin, S., Chen, M., Li, J., Lu, Z., Wang, N., Li, L., 2020. Preparation and performances characterization of HNIW/NTO-based high-energetic low vulnerable polymer-bonded explosive. J. Therm. Anal. Calorim. 139, 3589–3602.

Lan, G., Zhang, G., Shen, J., Li, Z., Wang, J., Li, J., 2022. Establishing the interface layer on the pentaerythritol tetranitrate surface *via in situ* reaction. Langmuir 38, 12016–12023.

Lan, G., Zhang, G., Chao, H., Li, Z., Wang, J., 2022. Jing Li, Ameliorating the performances of 3,4-bis(4′ -nitrofurazano-3′ -yl)furoxan (DNTF) by establishing tannic acid (TA) interface layer on DNTF surface. Chem. Eng. J. 434, 134513.

Li, S., Wang, J., Fu, X., Zhou, J., 1993. The research on some NTO salts used for energetic combustion catalyst. Chin. J. Energ. Mater. 3, 22–27.

Li, Z., Zhao, X., Gong, F., Lin, C., Liu, Y., Yang, Z., Nie, F., 2020. Multilayer deposition of metal-phenolic networks for coating of energetic crystals: modulated surface structures and highly enhanced thermal stability. ACS Appl. Energy Mater. 3, 11091–11098.

Liu, S., Du, B., Zhang, J., Pan, B., Li, W., Xie, G., 2001. Applied studies of new energetic catalysts in the screw extruded energetic propellant with low signature. Chin. J. Energ. Mater. 9, 130–131.

Liu, J., Ke, X., Xiao, L., Hao, G., Rong, Y., Jin, C., Jiang, W., Li, F., 2018. Application and properties of nano-sized RDX in CMDB propellant with low solid content. Propell. Explos. Pyrot. 43, 144–150.

Ren, T., 1994. Nitramine and nitrate ester explosives technology. China Weapons Industry Press, Beijing.

Ren, X., Li, M., Qiu, L., Guo, X., Tian, F., Han, G., Yang, W., Yu, Y., 2023. Cationic vacancies and interface engineering on crystalline–amorphous gamma-phase Ni–Co oxyhydroxides achieve ultrahigh mass/areal/ volumetric energy density flexible all-solid-state asymmetric supercapacitor. J. Mater. Chem. A 11, 5754–5765.

Sánchez-Martín, J., Beltrán-Heredia, J., Gibello-Pérez, P., 2011. Adsorbent biopolymers from tannin extracts for water treatment. Chem. Eng. J. 168, 1241–1247.

Singh, G., Kapoor, I.P.S., Felix, S.P., 2002. Studies on energetic compounds part 23: Preparation, thermal and explosive characteristics of transition metal salts of 5-nitro-2,4-dihydro-3H-1,2,4-triazole-3-one(NTO). Propell. Explos. Pyrot. 27, 16–22.

Song, N., Liu, J., Yang, L., Liu, P., 2020. Preparation of nano-spherical Cu-en and its catalytic study on the performance of solid propellant. Propell. Explos. Pyrot. 45, 1799–1804.

Stepanov, V., Willey, T.M., Ilavsky, J., Gelb, J., Qiu, H., 2013. Structural characterization of RDX-based explosive nanocomposites. Propell. Explos. Pyrot. 38, 386–393.

Sun, H., 1998. An ab initio force-field optimized for condensedphase applications overview with details on alkane and benzene compounds. J. Phys. Chem. B 102, 7338–7364.

Wu, K., Song, L., Wang, Z.Z., Hu, Y., 2008. Microencapsulation of ammonium polyphosphate with PVA-melamine-formaldehyde resin and its flame retardance in polypropylene. Polym. Adv. Technol. 19, 1914–1921.

Xiao, F., Liang, T., 2021. Preparation of hierarchical core-shell Al-PTFE@TA and Al-PTFE@TA-Fe architecture for improving the combustion and ignition properties of aluminum. Surf. Coat. Tech. 412, 127073.

Xiao, F., Liu, Z., Liang, T., Yang, R., Li, J., Luo, P., 2021. Establishing the interface layer on the aluminum surface through the self-assembly of tannic acid (TA): improving the ignition and combustion properties of aluminum. Chem. Eng. J. 420, 130523.

Yang, Z., Ding, L., Wu, P., Liu, Y., Nie, F., Huang, F., 2015. Fabrication of RDX, HMX and CL-20 based composites via in situ polymerization of melamineformaldehyde resins with reduced sensitivity. Chem. Eng. J. 268, 60–66.

Yuan, Z., Zhao, F., Jiao, J., Zhang, J., Yang, L., Zheng, X., Zhang, C., Xie, B., 2014. Effect of 2,4-dihydroxybenzoate lead/cupric on combustion properties of Al/RDX-CMDB propellants. Initiat. Pyrotech. 4, 20–23.

Zhang, X., Gao, M., Qiu, L., Sheng, J., Yang, W., Yu, Y., 2023. Sulfur vacancies-induced "Electron Bridge" in Ni_4Mo/Sv-$Zn_xCd_{1-x}S$ regulates electron transfer for efficient H_2-releasing photocatalysis. J. Energy Chem. 79, 64–71.

Zhang, M., Zhao, F., Li, H., Yuan, Z., Dong, S., Wang, Y., Chen, X., Yang, Y., Song, X., Jiang, Z., 2022. Insight into graphene-salen metal nanocomposites on combustion performance and mechanism of HMX-CMDB propellant. Chem. Eng. J. 429, 132175.

Zhao, C.Y., Zhang, G.H., 2011. Review on microencapsulated phase change materials (MEPCMs): fabrication, characterization and applications. Renew. Sust. Energ. Rev. 15, 3813–3832.